8-2021

Zernike Integrated Partial Phase Error Reduction Algorithm

Stephen C. Cain
Air Force Instittute of Technology

Recommended Citation

Cain, S. C. (2021). Zernike integrated partial phase error reduction algorithm. Results in Optics, 4, 100085. https://doi.org/10.1016/j.rio.2021.100085

Results in Optics 4 (2021) 100085

Contents lists available at ScienceDirect

Results in Optics

journal homepage: www.elsevier.com/locate/rio

Zernike integrated partial phase error reduction algorithm

Stephen C. Cain

Department of Electrical and Computer Engineering, Air Force Institute of Technology, 2950 Hobson Way, WPAFB, OH 45433, USA

ARTICLE INFO

Keywords:
Phase retrieval
Zernike polynomials
Blind deconvolution

ABSTRACT

A modification to the error reduction algorithm is reported in this paper for determining the prescription of an imaging system in terms of Zernike polynomials. The technique estimates the Zernike coefficients of the optical prescription as part of a modified Gerchberg-Saxton iteration combined with a new gradient-based phase unwrapping algorithm. Zernike coefficients are updated gradually as the error reduction algorithm converges by recovering the partial pupil phase that differed from the last known pupil phase estimate. In this way the wrapped phase emerging during each iteration of the error reduction algorithm does not represent the entire wrapped phase of the pupil electric field and can be unwrapped with greater ease.

The algorithm is tested in conjunction with a blind deconvolution algorithm using measured laboratory data with a known optical prescription and is compared to a baseline approach utilizing a combination of the error reduction algorithm and a least-squares phase unwrapper previously reported in the literature. The combination of the modified error reduction algorithm and the new least-squares Zernike phase unwrapper is shown to produce superior performance for an application where it is desirable that Zernike coefficients be estimated during each iteration of the blind deconvolution procedure.

1. Introduction

Phase retrieval techniques have, historically, been used with some success for determining the optical prescription of an imaging system (Fienup, 2013). The phase retrieval algorithm described in his paper is designed to determine the prescription of an optical system from a beacon. This is accomplished by unwrapping the phase of an estimated electric field in the pupil plane into a function described by the Zernike polynomials as it is estimated incrementally by an error reduction algorithm (Gerchberg and Saxton, 1972). This is accomplished by the Zernike Integrated Partial Phase Error Reduction (ZIPPER) approach, which is designed to constrain the shape of the estimated Point Spread Function (PSF) on each iteration as it is estimated from the images. This has the potential advantage for blind deconvolution algorithms where the shape of the object is being determined on an iterative basis and it is advantageous to constrain the shape of the PSF so as to avoid solutions of the image that could be arrived at through the use of estimated PSF shapes that are inconsistent with likely physical models.

Dealing with extended sources is important for problems where it is desirable to recover the optical aberrations of a system when presenting it with an optical source that is not sufficiently small to be considered a points source. This is potentially valuable when viewing laser guide star beacons, which often are spatially too large to be considered point sources. The proposed technique will be shown to be useful for recovering the optical prescription of the system from the full aperture but could theoretically be applied to wave front sensor observations to recover the phase over individual sub-apertures.

Other phase retrieval methods for fitting a Zernike polynomial basis to the aberrations of an optical system include curvature sensing, the Gerchberg-Saxton (GS) algorithm combined with phase unwrapping algorithms and intensity based least squares fitting (Roddier, 1988; Krist and Burrows, 1995). Attempts continue to be made to produce reliable 2-D phase unwrapping algorithms, but their performance continues to be limited by branch cuts and noise as will be demonstrated in this paper (Ghiglia and Pritt, 1998; Xia et al., 2016). Krist et al successfully used a Levenberg-Marquardt (LM) least-squares method to determine the Zernike coefficients for the aberrations in the Hubble Space Telescope (Krist and Burrows, 1995). One limitation of this technique is that it required them to decouple the aberrations by defocusing the telescope. Their strategy involved determining the lower order aberrations first, which allowed the remaining phase error to be retrieved using GS phase retrieval with a small enough amplitude that it did not require to be unwrapped (Krist and Burrows, 1995).

Roddier's curvature sensing technique also determines low-order aberrations by defocusing the image of a point source that can be used to estimate to Zernike polynomials coefficients (Roddier, 1988). Phase diversity is a multi-image strategy that most commonly incorporates

E-mail address: Stephen.Cain@afit.edu

https://doi.org/10.1016/j.rio.2021.100085
Received 3 February 2021; Revised 25 March 2021; Accepted 30 March 2021

defocused images combined with in focus images to facilitate phase retrieval (Paxman et al., 1992). A single plane out of focus method for curvature sensing was also developed by Hickson and was used in the alignment process for a large telescope (Woods, 2012; Hickson, 1994; Tokovinin and Heathcote, 2006). In contrast to these some other methods, ZIPPER does not require gradient searches through multi-dimensional Zernike coefficient space as in (Krist and Burrows, 1995; Zingarelli and Cain, 2013) and can utilize the speed advantages of the Gerchburg-Saxton phase retrieval algorithm while still allowing for unwrapped phase estimates to be obtained.

This paper is organized as follows: Section 2 will describe the experimental setup used to generate an optical system with known aberrations. Section 3 will introduce the optical system model and serve to show how the known aberration coefficients are computed. Section 4 will cover the algorithm used to process the image data obtained from the experimental setup. Section 5 will contain results obtained from the new algorithm and a baseline approach on the experimental datasets and Section 6 will present conclusions and discuss future research.

2. Experimental setup

In this section, an experiment that measures the PSF of an optical system possessing an astigmatism aberration that is the result of a plane wave entering from a point that is 7.2 degrees from the optic axis is described (Zingarelli and Cain, 2013). The optical arrangement is chosen to be simple enough to realize with widely available optical components, yet the configuration is chosen to produce an aberration that is commonly modeled using geometric optics (Hecht, 1990). This aberration is of general interest since it can serve to limit the useful field of view of an optical telescope and would interact with atmospheric aberrations in ways difficult to predict with ray tracing techniques. Fig. 1 shows the optical arrangement in which the lens has a 1 cm diameter and has a focal length of 50 cm.

Fig. 1 shows the optical arrangement with the light emitting diode 22.3 cm off the optic axis and 1.78 m in front of the lens, which is labeled as S1. The image point for the light emitting diode is 68 cm behind the center of the lens and is labeled as the distance S2. The positive, negative and in focused images are collected with the camera 2.85 cm ahead, 3.25 cm behind the image point respectively. The camera is a 512 X 512 Princeton Instruments Cascade model possessing with a 16 μm pixel pitch. Figs. 2 and 3 show a sample image taken from a 100 frame sequence of image data gathered at the positive and negative focus image positions (200 frames in all). Fig. 4 shows the 100 frame average of the in focus image for reference.

3. Optical system model

The PSF of an optical system can be modeled via the Rayleigh-Sommerfeld diffraction formula as shown below (Goodman, 1968).

$$U(\xi,\eta,z)=\frac{z}{j\lambda}\int_x\int_y U(x,y,0)\frac{e^{j2\pi R(x,y,\xi,\eta)/\lambda}}{R^2(x,y,\xi,\eta)}dxdy \tag{1}$$

The Rayleigh-Sommerfeld diffraction equation relates the source field, U(x,y,)0)in the pupil to the receiver field U(ξ,η,z) in the focal plane. In Eq. (1), z is the perpendicular distance between the source and receiver planes while R is the distance between a point in the pupil, (x,y), and a point on the receiver plane, (ξ,η). The source is assumed to be monochromatic with wavelength λ.

The distance R is computed using the discrete form found in Eq. (2),

$$R(n,m,k,l)=\sqrt{(n\Delta_r-k\Delta_s)^2+(m\Delta_r-l\Delta_s)^2+z^2} \tag{2}$$

where Δ_r is the sample size in the receiver plane, Δ_s is the sample size in the pupil plane, (n,m) are pixel coordinates in the receiver plane and (k, l) are discrete coordinates in the pupil plane. Eq. (1) can be simplified without loss of fidelity by approximating R with z (Goodman, 1968). With these substitutions, Eq. (1) becomes:

$$U_r(n,m)\approx\frac{\Delta_s^2}{j\lambda}\sum_{k,l}U_s(k,l)\frac{e^{j2\pi R(n,m,k,l)/\lambda}}{z} \tag{3}$$

The source field presented to the lens, U_s, is computed using a simple spherical wave model with a lens transformation for a simple spherical lens added to the phase of the field (Goodman, 1968). Since the PSF is being computed, the source is modeled as producing an expanding spherical wave as shown in Eq. (4).

$$U_s(k,l)=\frac{S_1 e^{\frac{j2\pi\sqrt{(k\Delta_s-x_s)^2+(l\Delta_s-y_s)^2+S_1^2}}{\lambda}}t_l(k,l)}{(k\Delta_s-x_s)^2+(l\Delta_s-y_s)^2+S_1^2} \tag{4}$$

In this equation x_s is 22.3 cm, and y_s is zero representing the position of the light source in front of the lens a distance of S_1 shown in Fig. 1 in front of the lens. The pupil is circular with a 1 cm in diameter. The lens transformation $t_l(k,l)$ is a place holder for both the phase transformation of the lens or mirrors and can accommodate additional terms that might be related to atmospheric turbulence. In this experiment it is modeled as a simple spherical lens with a focal length of 50 cm (Goodman, 1968).

The phase in the pupil computed to the center pixel of the PSF can be computed as the phase imparted by the incoming spherical wave plus the lens transformation phase and the phase term generated by the Rayleigh-Sommerfeld propagation from the pupil to the center pixel at (n,m) = (0,0). The sum of all three phases is shown in Eq. (5).

$$\theta_{tot}(k,l)=\frac{2\pi\sqrt{(k\Delta_s-x_s)^2+(l\Delta_s-y_s)^2+S_1^2}}{\lambda}+\theta_{lens}(k,l)+2\pi R(0,0,k,l)/\lambda, \tag{5}$$

where θ_{lens} is the phase of the lens transformation. The number of points chosen to model the pupil is 1558 making the sample size in the pupil 6.42 μm.

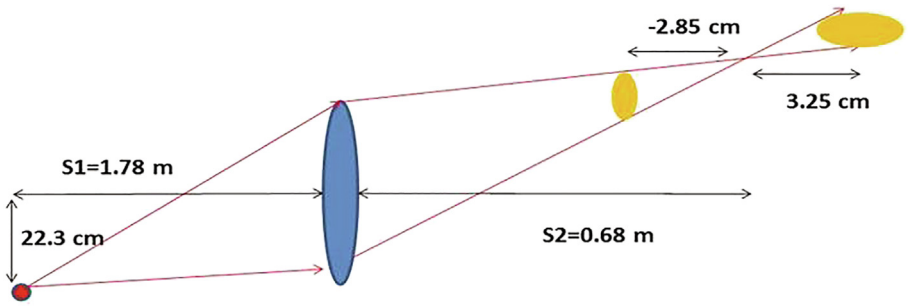

Fig. 1. Optical arrangement used to produce an astigmatism aberration (elliptical spots shown before and after the focal point). The wavelength of the light is 0.648 μmeters.

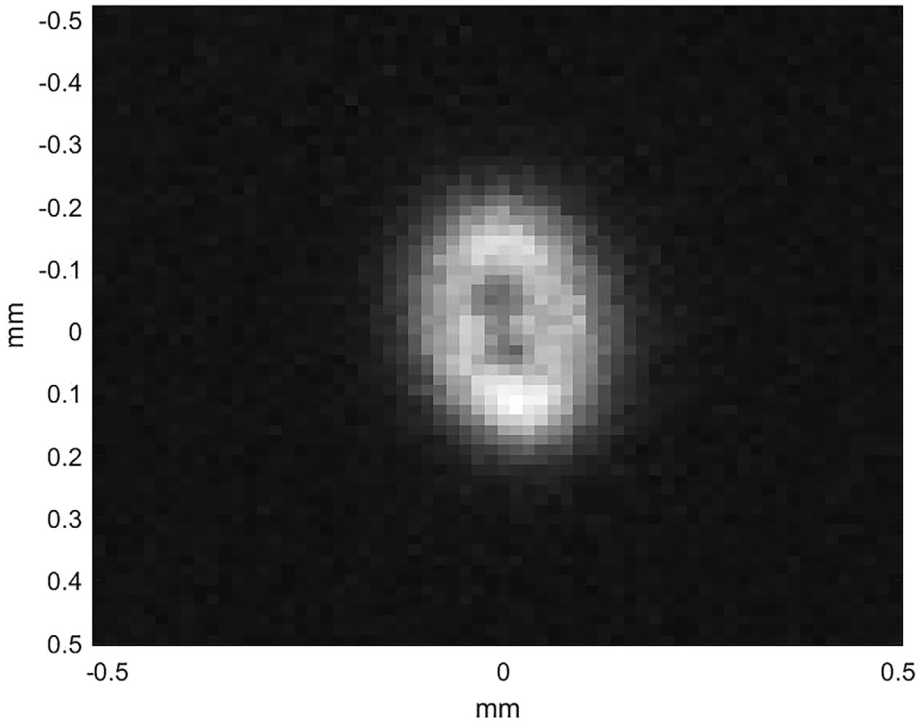

Fig. 2. Image of a 75 μm pinhole back illuminated by a red LED for the positive defocus case.

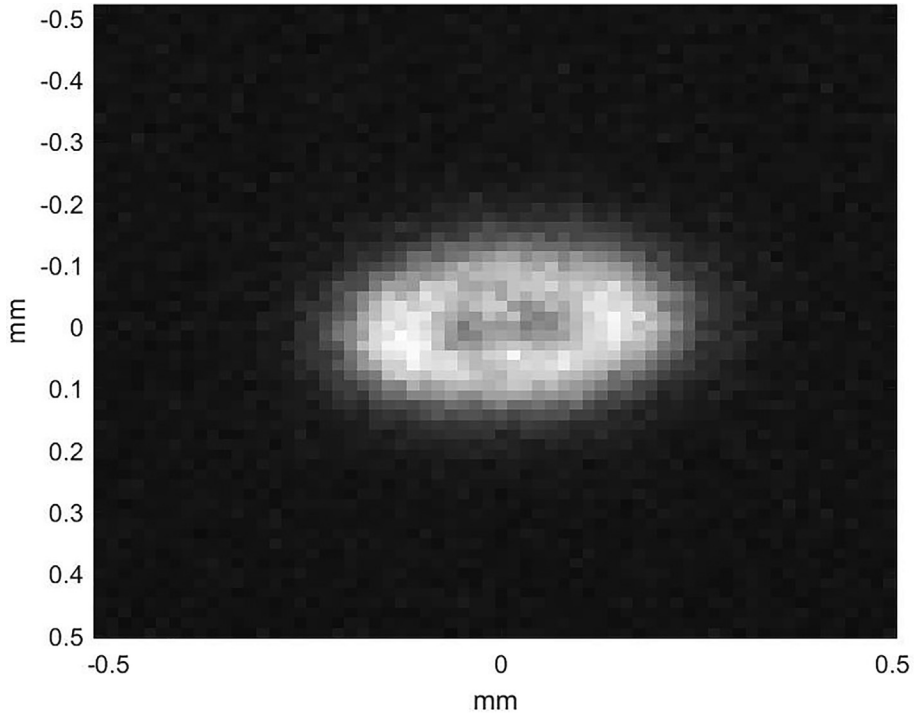

Fig. 3. Image of a 75 μm pinhole back illuminated by a red LED for the negative defocus case.

The PSF of the system is shown in Figs. 5–7 for the positive, negaitve and in focus cases respectively. All the PSF images are rotated by 7.2 degrees to match measured images. Table 1 shows the aberration coefficients for the in focus and out of focus cases obtained by decomposing the phase computed in Eq. (5) into Zernike coefficients. This simulated phase is not wrapped and is therefore simple to convert into aberration coefficients shown in Table 1 using a method found in (Zingarelli and Cain, 2013).

4. Image processing algorithms

The algorithms utilized in this paper for processing the image data described previously fall into three different categories which will be described in order of their utilization. The first is a blind deconvolution algorithm, which is used to recover estimates of the point spread functions (PSFs) from the image data. The second is a phase retrieval algorithm that is integrated as a step in the blind deconvolution proce-

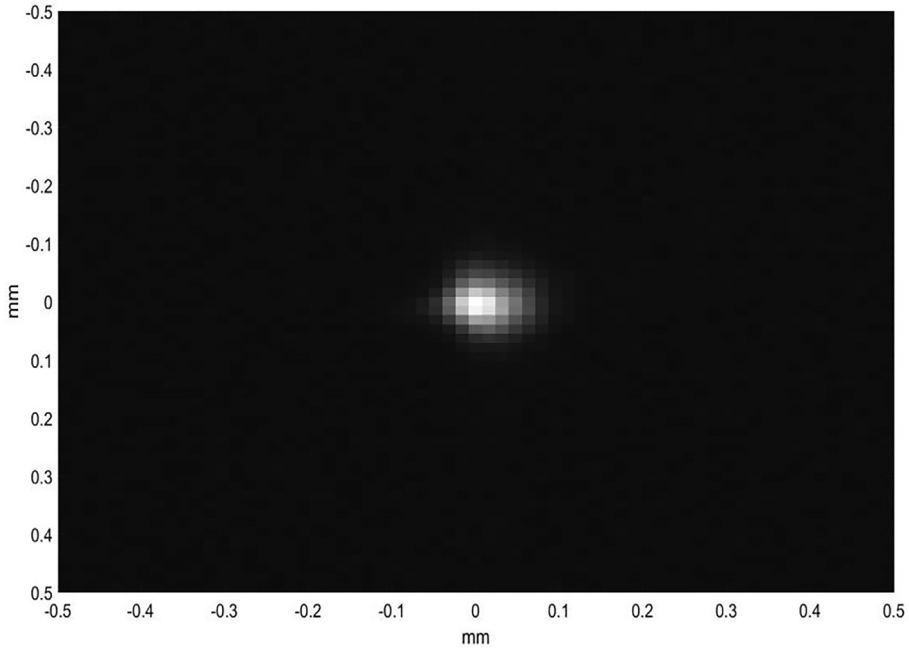

Fig. 4. Image of a 75 μm pinhole back illuminated by a red LED for the in-focus case.

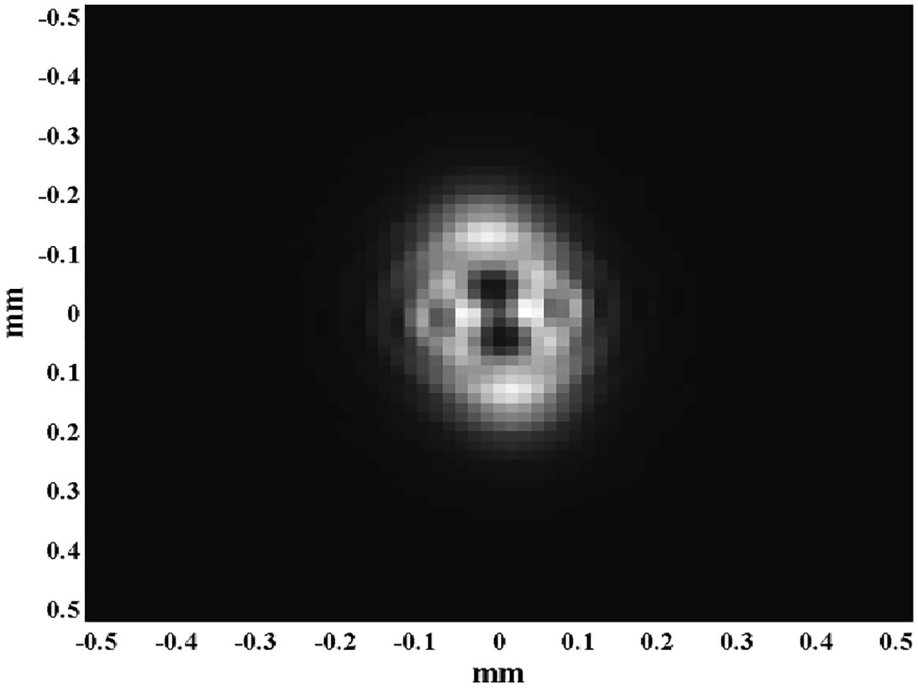

Fig. 5. Image of the PSF simulated using the Rayleigh-Sommerfeld diffraction formula for the positive defocus case.

dure. This paper introduces a new approach for phase retrieval that contains a modified version of the error reduction algorithm. The modification described in this chapter will show how the differential phase between the last estimate of the Zernike coefficients and the new one is obtained. This differential phase is prone to contain less wrapping than the entire phase and so is then fed into the third type of algorithm discussed in this paper, which is a phase unwrapping algorithm. In this paper, a new phase unwrapping algorithm is introduced that is part of the ZIPPER approach. This new phase unwrapping algorithm is compared to that of a baseline approach previously reported in the literature (Xia et al., 2016).

The modified error reduction algorithm, together with the new phase unwrapping approach, constitute the ZIPPER algorithm, which will be compared to a the standard Gerchberg-Saxton phase retrieval algorithm combined with a phase unwrapping step using the CPULSI phase unwrapper. Each of these approachs will work to constrain the phase estimates to a set of Zernike coefficients on each iteration of the blind deconvolution algorithm. Entirely different results may be obtained by running the full blind deconvolution algorithm without phase unwrapping and unwrapping the phase at the end, but the phase will not be constrained on each iteration, so any method not recovering Zernike coefficients on each iteration cannot claim to estimate Zer-

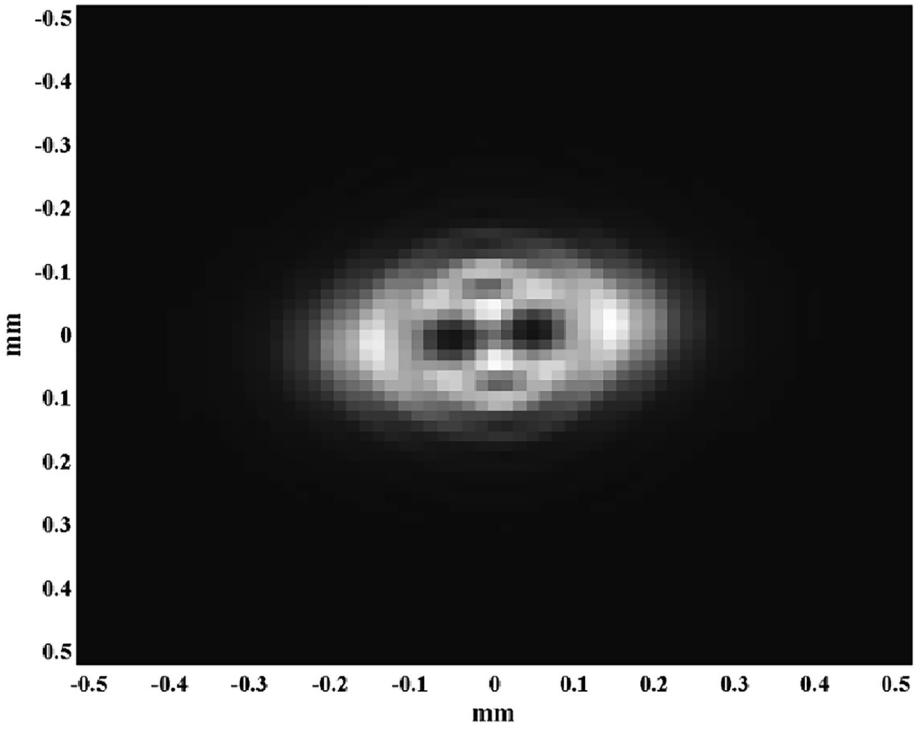

Fig. 6. Image of the PSF simulated using the Rayleigh-Sommerfeld diffraction formula in the negative defocus case.

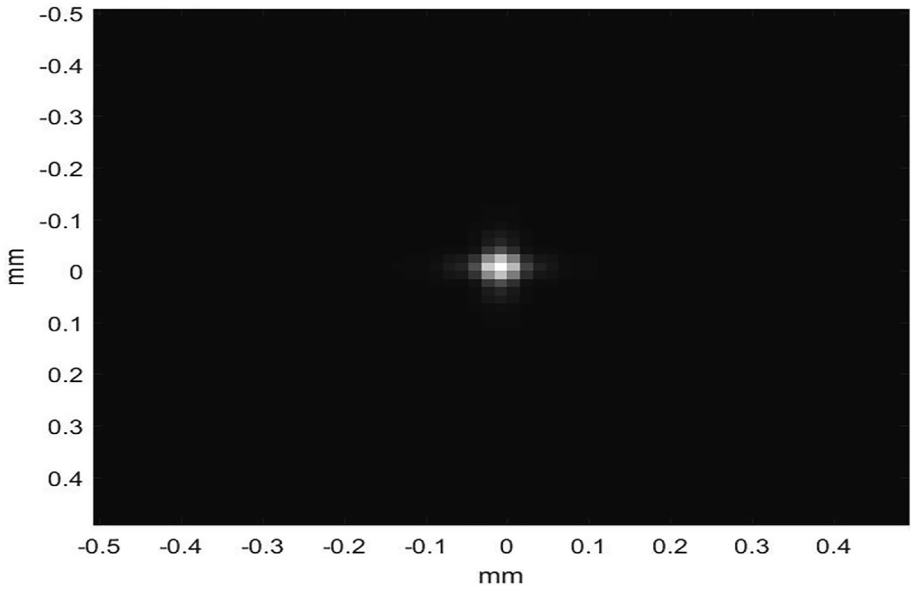

Fig. 7. Image of the PSF simulated using the Rayleigh-Sommerfeld diffraction formula for the in-focus case.

Table 1
Aberration coefficients obtained by analyzing the phase error computed from Eq. (5) for the out of focus cases of negative and positive focus images.

Focus	Z4	Z5	Z6	Z7	Z8	Z9	Z10	Z11
Negative	−2.41	−0.01	−0.74	−0.02	−0.03	0.00	0.00	−0.03
Positive	2.09	−0.01	−0.78	−0.02	−0.03	0.00	0.00	−0.03

nike coefficients iteratively and therefore will not be considered as a candidate for comparison in this study since the goal of this research is to create a image recovery algorithm that constrains the phase error to be parameterized over a set of Zernike polynomials while estimating the shape of the object.

4.1. Blind deconvolution algorithm

The model for the photo detector array assumes the response of the detectors is uniform from pixel to pixel as is the bias. In practice non-uniform factors should be calibrated out of the measured data to pro-

vide estimates of the number of photons collected by each element in the array (Stephen, 2020). The number of photoelectrons measured at each detector in the array is assumed to be a Poisson random variable with a mean equal to the sum of the mean number of photons from the objects in the field of view and the background

The data from these sources is modeled as separate Poisson random variables such that the data from the objects, $d_k(z, w,x,y)$, has the mean show in Eq. (6).

$$E[d_k(z,w,x,y)] = \gamma_k o(x,y) h_k(z-x, w-y) \tag{6}$$

In this Equation, (x,y) are coordinates in the object plane, (z,w) are coordinates in the detector plane, o is the image containing the objects in the scene, γ_k is the number of photo-electrons from optical sources in the k'th frame of image data out of a total of J frames and h_k is the PSF in the k'th frame. The second set of data. $d_B(z, w,k)$ has a mean equal to the background level as shown in Eq. (7).

$$E[d_B(z,w,k)] = B_k \tag{7}$$

In this equation, B_k is the background level in the k'th frame of data, which is assumed to be uniform in the field of view on average and is computed using a median filter. The measured data, $\tilde{d}_k(z,w)$ is also Poisson and is equal to the sum of all both data sets as shown in Eq. (8).

$$\tilde{d}_k(z,w) = \sum_{x=1}^{M}\sum_{y=1}^{M} d_k(z,w,x,y) + d_B(z,w,k) \tag{8}$$

An Expectation-Maximization approach is adopted for computing the image of an unknown object and the associated point spread functions from multiple frames of camera data (Schulz, 1993; Dempster et al., 1977; Shepp and Vardi, 1982). This procedure begins by identifying the joint log-likelihood of the two data sets, $d_k(z, w,x,y)$ and $d_B(z, w,k)$. Since these data are assumed to be Poisson and both statistically independent from one another as well as statistically independent from pixel to pixel, the joint log-likelihood, $L(o,h,\gamma_{kk})$, can be expressed using the following equation, which assumes that both the object and the PSF's each sum to one and the data in each pixel in every frame are statistically independent from one another:

$$\begin{aligned} L(o,h_k,\gamma_k) = &\sum_{k=1}^{J}\sum_{z=1}^{M}\sum_{w=1}^{M}\sum_{x=1}^{M}\sum_{y=1}^{M}[d_k(z,w,x,y)\ln(\gamma_k o(x,y)h_k(z-x,w-y))] \\ &-\sum_{k=1}^{L}\sum_{z=1}^{M}\sum_{w=1}^{M}\sum_{x=1}^{M}\sum_{y=1}^{M}[\ln(d_k(z,w,x,y)!)\ )] \ -\sum_{k=1}^{N}\gamma_k \end{aligned} \tag{9}$$

In order to simplify the solution process, the log-likelihood will be maximized with respect to the image o(x,y), the photon-count value in each frame, $_k$ and the PSF in each frame h_k, then the conditional expected value of the result will be computed given the measured data $\tilde{d}_k(z,w)$ in a way similar to other blind deconvolution algorithms (Schulz, 1993; Dempster et al., 1977).

The derivative of $L(o,h_k,\gamma_k)$, with respect to γ_k is computed as shown in Eq. (10) assuming that both the object, o and PSFs, h_k sum to one.

$$\frac{dL(o,h_k,g_k)}{d\gamma_k} = \sum_{z=1}^{M}\sum_{w=1}^{M}\sum_{x=1}^{M}\sum_{y=1}^{M}\frac{d_k(z,w,x,y)}{\gamma_k} - 1 \tag{10}$$

A second derivative yields a strictly negative result, implying that a solution for Eq. (10) when the derivative is set equal to zero will produce a maximum of the log-likelihood function. The solution for γ_k that maximizes $L(o,h_k,\gamma_k)$ is shown in Eq. (11). The conditional mean of the estimate given the measured data is computed to show the form of the estimate obtained from the Expectation-Maximization process.

$$\gamma_k = \sum_{z=1}^{M}\sum_{w=1}^{M}\sum_{x=1}^{M}\sum_{y=1}^{M} E[d_k(z,w,x,y)|\ \tilde{d}_k(z,w)] \tag{11}$$

The expectation step shown in Eq. (11) is necessary since the data described in Eq. (6) is not directly observable but is contained within the observed data, $\tilde{d}_k(z,w)$ as shown in Eq. (8). The conditional expectation has been solved by Shepp and Vardi and is substituted into Eq. (11) to yield the following result (Shepp and Vardi, 1982).

$$\gamma_k^{new} = \gamma_k^{old}\sum_{z=1}^{M}\sum_{w=1}^{M}\frac{\sum_{x=1}^{M}\sum_{y=1}^{M} o^{old}(x,y)h_k^{old}(z-x,w-y)\tilde{d}_k(z,w)}{\sum_{x=1}^{M}\sum_{y=1}^{M} o^{old}(x,y)h_k^{old}(z-x,w-y)+B_k} \tag{12}$$

In this equation a variable with the *old* superscript denotes a quantity computed with estimates obtained from the previous iteration of the EM algorithm. γ_k^{new} denotes the new estimate obtained from the EM algorithm for the number of photons present in the k'th data frame. In this way the algorithm is implemented by the user providing a starting estimate which is updated from iteration to iteration via Eq. (12). One obvious way to initialize the estimate for γ_k is to subtract the median value, B_k, from the image, $\tilde{d}_k(z,w)$, and sum the result over all pixels.

In order to solve for the object function, o(x,y), The derivative of $L(o,h_k,\gamma_k)$, with respect to a specific point in the image $o(x_o,y_o)$ is computed as shown in Eq. (13) assuming that the PSF, h_k sums to one. The method of Lagrange is implemented in order to force the object to sum to one. The derivative of the constraint function, $\theta\sum_{x=1}^{M}\sum_{y=1}^{M} o(x,y)$ is subtracted from the derivative of the log-likelihood function, where θ is the Lagrange multiplier (Schulz, 1993).

$$\frac{\partial L(o,h_k,g_k)}{\partial o(x_o,y_o)} - \frac{\partial\theta\sum_{x=1}^{M}\sum_{y=1}^{M} o(x,y)}{\partial o(x_o,y_o)} = \sum_{z=1}^{M}\sum_{w=1}^{M}\frac{d_k(z,w,x_o,y_o)}{o(x_o,y_o)} - \theta \tag{13}$$

The solution for $o(x_o,y_o)$ that maximizes $L(o,h_k,\gamma_k)$ subject to the constraint that o(x,y) sums to one is shown in Eq. (14) by setting Eq. (13) equal to zero and solving for $o(x_o,y_o)$. The conditional mean of the estimate given the measured data is computed to show the final form of the estimate obtained from the Expectation-Maximization process.

$$\begin{aligned} o(x_0,y_o)^{new} = &\ o^{old}(x_o,y_o)\sum_{k=1}^{L}\sum_{z=1}^{M}\sum_{w=1}^{M} \\ &\times\frac{h_k^{old}(z-x_o,w-y_o)\tilde{d}_k(z,w)}{\theta\sum_{x=1}^{M}\sum_{y=1}^{M} o^{old}(x,y)h_k^{old}(z-x,w-y)+B_k} \end{aligned} \tag{14}$$

In this paper the image o(x,y) is initialized as being equal to one within a circular region corresponding to the size of the aperture used to generate the source for the images. The Lagrange multiplier serves to provide a factor that can be adjusted to force the image to sum to one. It is utilized this way in the algorithm, being applied as the appropriate scale factor to force this condition on each iteration of the algorithm.

Finally, the solution for the PSF is obtained by computing the derivative of $L(o,h_k,\gamma_k)$, with respect to a specific point in the PSF $h_k(x_o,y_o)$ as shown in Eq. (15) assuming that the object, o(x,y) sums to one. The method of Lagrange is implemented once again in order to force the PSF to sum to one. The derivative of the constraint function, $\theta_k\sum_{x=1}^{M}\sum_{y=1}^{M} h_k(x,y)$ is subtracted from the derivative of the log-likelihood function, where θ_k is the Lagrange multiplier.

$$\begin{aligned} &\frac{\partial L(o,h_k,g_k)}{\partial h_k(x_o,y_o)} - \frac{\partial\theta_k\sum_{x=1}^{M}\sum_{y=1}^{M} h_k(x,y)}{\partial h_k(x_o,y_o)} \\ &= \sum_{z=1}^{M}\sum_{w=1}^{M}\frac{d_k(z,w,z-x_o,z-y_o)}{h_k(x_o,y_o)} - \theta_k \end{aligned} \tag{15}$$

The solution for $h_k(x_o,y_o)$ that maximizes $L(o,h_k,\gamma_k)$ subject to the constraint that $h_k(x,y)$ sums to one is shown in Eq. (16) by setting Eq. (15) equal to zero and solving for $h_k(x_o,y_o)$. The conditional mean

of the estimate given the measured data is computed to show the final form of the estimate obtained from the Expectation-Maximization process.

$$h_k^{new}(x_0,y_o) = h_k^{old}(x_o,y_o)\sum_{z=1}^{M}\sum_{w=1}^{M} \times \frac{o_k^{old}(z-x_o,w-y_o)\tilde{d}_k(z,w)}{\theta_k\sum_{x=1}^{M}\sum_{y=1}^{M}o^{old}(x,y)h_k^{old}(z-x,w-y)+B_k} \quad (16)$$

In this paper the PSFs $h_k(x,y)$ are initialized as being equal to a PSF generated with a single defocus aberration of Z_4 equal to 1 or -1, depending on whether the image in the k'th frame is collected within the positive or negative focus position. The frame taken at the in-focus position is initialized with a positive focus aberration $Z_4 = 1$.

At each iteration γ_k^{new},h_k^{new}, and o^{new} are computed from old estimates. Before going into the next iteration, the phase retrieval step described in the next subsection is executed.

4.2. Phase retrieval algorithm

The ZIPPER approach used to recover the pupil field from h_k^{new} is a modification of the Gerchberg-Saxton phase retrieval algorithm. Entering each iteration, not only is h_k^{old} known, but also the Zernike coefficients [α_{k4}^{old}, $\alpha_{k,5}^{old}$, $\alpha_{k,6}^{old}$,…., $\alpha_{k,N}^{old}$] associated with the k'th PSF. In this paper, N is chosen to be 11, to allow for reconstruction of the phase, but to provide ample constraints to prevent the PSFs from matching the noise features (Zingarelli and Cain, 2013). The phase $\phi_k(u,v)$ is computed from (N-3) Zernike coefficients via the formula,

$$\phi_k^{old}(u,v) = \sum_{i=4}^{N}\alpha_{k,i}^{old}Z_i(u,v) \quad (17)$$

The first three Zernike terms are not considered as they don't affect the PSF shape (Goodman, 1968). This pupil phase is combined with the known clear aperture function A(u,v) to form an estimate of the sampled detector field, $f_k$via the Eq. (18) (Gerchberg and Saxton, 1972);

$$f_k(x,y) = \sum_{u=1}^{M}\sum_{v=1}^{M}A(u,v)e^{j\phi_k(u,v)}e^{j2\pi(ux+vy)/M} \quad (18)$$

The amplitude of this field is replaced with the square root of h_k^{new} to produce a new detector field, $\tilde{f}_k$, via Eq. (19) (Gerchberg and Saxton, 1972);

$$\tilde{f}_k(x,y) = \sqrt{h_k^{new}(x,y)}e^{j\arg(f_k(x,y))} \quad (19)$$

In this Equation arg() stands for the angle of the complex number that is its argument. After this replacement, a new pupil field, $g_k(u,v)$ is computed from Eq. (20) (Gerchberg and Saxton, 1972);

$$g_k(u,v) = \sum_{x=1}^{M}\sum_{y=1}^{M}\tilde{f}_k(x,y)e^{-j2\pi(ux+vy)/M} \quad (20)$$

Now, $g_k(u,v)$ is the field in the pupil and we wish to replace its magnitude with the known clear aperture function, A(u,v). To do this we must recover the angle of the complex field at every point (u,v) in the pupil plane in much the same was as we did with the field in the detector $f_k(x,y)$ by using the arg() function (Gerchberg and Saxton, 1972).

The modification proposed to the Gerchberg-Saxton algorithm is to take the argument of the field $g_k(u,v)$ times the conjugate of phasor constructed from the old Zernike coefficients as shown in Eq. (21).

$$\tilde{\phi}_k(u,v) = \arg(g_k(u,v)e^{-j\phi_k^{old}(u,v)}) \quad (21)$$

In this Equation, $\tilde{\phi}_k(u,v)$ represents the phase difference between the new phase recovered by the Gerchberg-Saxton error reduction algorithm in the pupil plane and the original phase in the pupil plane from the previous iteration of the Gerchberg-Saxton algorithm. It has the benefit of only representing the phase change accomplished by the Gerchberg-Saxton algorithm since the last iteration, thus potentially making it easier to unwrap, since the changes are most likely smaller than the total phase of the pupil field.

There are two phase unwrapping algorithms explored in this paper. The first is the CPULSI (Calibrated Phase Unwrapping based on Least-Squares and Iterations) phase unwrapper which is used together with the Gerchberg-Saxton algorithm in the baseline approach (Xia et al., 2016). It produces an unwrapped phase, $\tilde{\phi}'_k(u,v)$ from the phase $\tilde{\phi}_k(u,v)$ and the known clear pupil function A(u,v). The new approach used as part of the ZIPPER method, uses a gradient descent algorithm for computing Zernike coefficients and accomplishing the phase wrapping (Bartelt, 2020). The model for the phase is,

$$\tilde{\phi}'_k(u,v) = \tilde{\phi}_k(u,v) + 2\pi K(u,v)$$

In this Equation, K is the wrapping function that relates the unwrapped phase to the wrapped phase. In order to estimate K, a mean squared error cost function is constructed.

$$\varepsilon_k = \sum_{u=1}^{M}\sum_{v=1}^{M}\left(\tilde{\phi}'_k(u,v) - \tilde{\phi}_k(u,v) - 2\pi K(u,v)\right)^2 \quad (22)$$

The first step in unwrapping the phase is to compute the Zernike coefficients [$\alpha'_{k,4}$, $\alpha'_{k,5}$, $\alpha'_{k,6}$,…., $\alpha'_{k,N}$] from the potentially wrapped phase, $\tilde{\phi}_k(u,v) - 2\pi K(u,v)$, using the method found in (Zingarelli and Cain, 2013). These Zernike coefficients are used to compute the current estimate of the unwrapped phase, $\tilde{\phi}'_k(u,v)$. In the first iteration, K is assumed to be zero everywhere. This unwrapped phase estimate is then substituted into Eq. (22) and the derivative of the error, ε_k, with respect to a single point in the pupil plane, $K(u_o,v_o)$, is computed,

$$\frac{\partial\varepsilon_k}{\partial K(u_o,v_o)} = -4\pi\sum_{u=1}^{M}\sum_{v=1}^{M}\left(\tilde{\phi}'_k(u,v) - \tilde{\phi}_k(u,v) - 2\pi K(u,v)\right) \quad (23)$$

If the absolute value of the gradient at each pixel in the pupil exceed $\pi/2$, then K is incremented by 1 or -1 depending on the sign of the derivative. With the new estimate of K, the process is repeated as shown in Fig. 8. It continues till the new K is equal to the old K. At that point the unwrapped phase is computed.

The unwrapped phase, $\tilde{\phi}'_k(u,v)$, is then decomposed into Zernike coefficients to recover [$\beta_{k,4}$, $\beta_{k,5}$, $\beta_{k,6}$,…., $\beta_{k,N}$], which are the Zernike coefficients associated with the differential phase $\tilde{\phi}_k(u,v)$. The new Zernike coefficients [$\alpha_{k,4}^{new} = \alpha_{k,4}^{old} + \beta_{k,4}$, $\alpha_{k,5}^{new} = \alpha_{k,5}^{old} + \beta_{k,5}$, $\alpha_{k,6}^{new} = \alpha_{k,6}^{old} + \beta_{k,6}$,…., $\alpha_{kk,N}^{new} = \alpha_{k,N}^{new} + \beta_{k,N}$] are then carried into the next iteration as the old Zernike coefficient estimates and the process repeats itself.

In this paper, the phase retrieval process was repeated 10 times for every iteration of the blind deconvolution algorithm. Once the Zernike coefficients are updated 10 times, they are used to compute the final version of the PSF, $h_k^{new}(x,y)$, that is used in the next iteration via Eq. (24) (Goodman, 1968).

$$h_k^{new}(x,y) = \left|\sum_{u=1}^{M}\sum_{v=1}^{M}A(u,v)e^{j\sum_{i=1}^{N}\alpha_{k,i}^{new}Z_i(u,v)}e^{-j2\pi(ux+vy)/M}\right|^2 \quad (24)$$

This new PSF is used to enter the next iteration and becomes the old PSF as the new Zernike coefficients become the old ones as illustrated in Fig. 8. The iterations proceed until the root mean squared difference between the new Zernike coefficients and the old ones over all frames, as shown in Eq. (25), is less than a threshold, which was set at 5e-4 in this paper. This threshold was chosen to be an order of magnitude lower than the number of significant figures reported in the results for the Zernike coefficients so as to be small enough to be inconsequential. If an algorithm failed to meet the convergence criterion, then it would terminate after 1000 iterations.

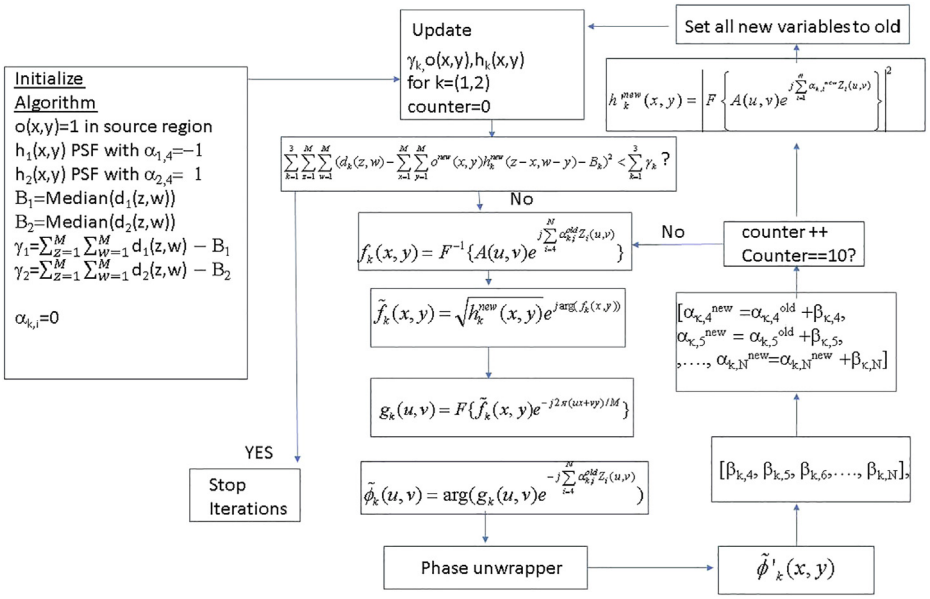

Fig. 8. Figure showing the flow of the combined blind deconvolution and phase retrieval algorithm.

Table 2
Average aberration coefficients obtained by analyzing the phase error computed using the two algorithmic approaches for the negative defocus image. The true Zernike coefficients were obtained from Table 1. The RMS error of the ZIPPER method is 0.16 waves. The GS-CPULSI method has an RMS coefficient error of 1.78 waves, almost 10 times higher than the ZIPPER method.

Focus	Z4	Z5	Z6	Z7	Z8	Z9	Z10	Z11
True	−2.41	−0.01	−0.74	−0.02	−0.03	0.00	0.00	−0.03
ZIPPER	−2.14	−0.01	−0.69	−0.06	0.07	0.03	0.02	0.29
GS + CPULSI	−1.05	0.01	−0.15	−0.28	0.54	−0.35	0.04	2.27

Table 3
Average aberration coefficients obtained by analyzing the phase error computed using the two algorithmic approaches for the nositive defocus images. The true Zernike coefficients were obtained from Table 1. The RMS error of the ZIPPER method is 0.1 waves. The GS-CPULSI method has an RMS coefficient error of 0.96 waves, almost 10 times higher than the ZIPPER method.

Focus	Z4	Z5	Z6	Z7	Z8	Z9	Z10	Z11
True	2.09	−0.01	−0.78	−0.02	−0.03	0.00	0.00	−0.03
ZIPPER	2.11	−0.02	−0.70	−0.09	0.07	0.01	0.01	−0.31
GS + CPULSI	1.04	−0.61	−0.25	0.83	0.13	0.14	−0.09	−2.26

Table 4
Aberration coefficient standard deviation obtained by analyzing the phase error computed using the two algorithmic approaches for all 200 images used to create the average images shown in Fig. 2 and 3. The ZIPPER algorithm possesses an average of nearly 1/10 the standard deviation of the GS-CPULSI method.

Focus	Z4	Z5	Z6	Z7	Z8	Z9	Z10	Z11
ZIPPER	0.05	0.02	0.06	0.01	0.02	0.01	0.01	0.16
GS + CPULSI	0.30	0.47	0.28	0.47	0.50	0.26	0.16	0.43

$$\sqrt{\sum_{k=1}^{K}\sum_{i=4}^{N}\left(\alpha_{k,i}^{new}-\alpha_{k,i}^{old}\right)^2/(K(N-3))} \tag{25}$$

5. Results

This section reports results obtained from processing image data described in Section 2 of this paper. First, 100 negative and positive defocus images, of which samples are shown in Figs. 2 and 3, were input into the algorithm and processed two different ways. One way was to use the ZIPPER algorithm with the new phase unwrapper, unwrapping the differential phase on every iteration of the Modified Gerchberg Saxton algorithm. The second method was to use traditional Gerchberg-Saxton phase retrieval and unwrap the phase after every iteration using the CPUlSI phase unwrapper (Xia et al., 2016).

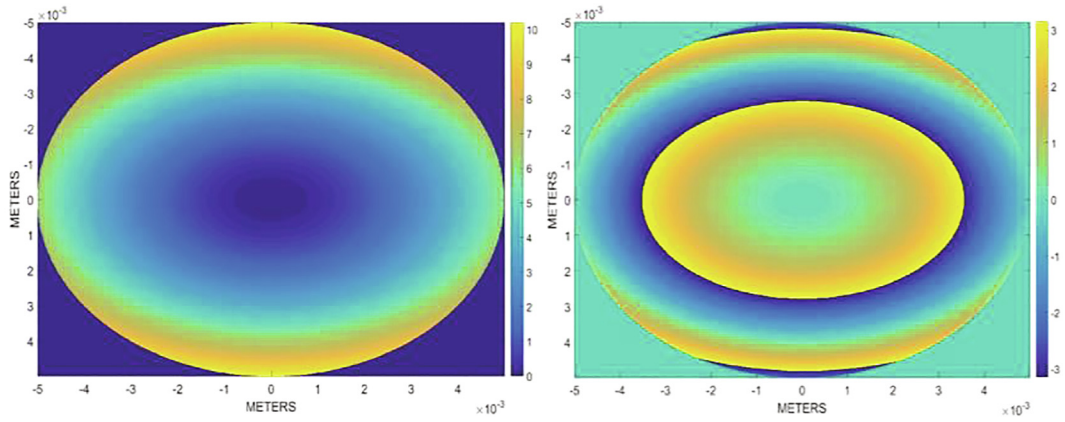

Fig. 9. Images of the unwrapped and wrapped phase recovered from the averaged positive defocus image. The color bar on the side is in units of radians demonstrating significant potential for phase wrapping.

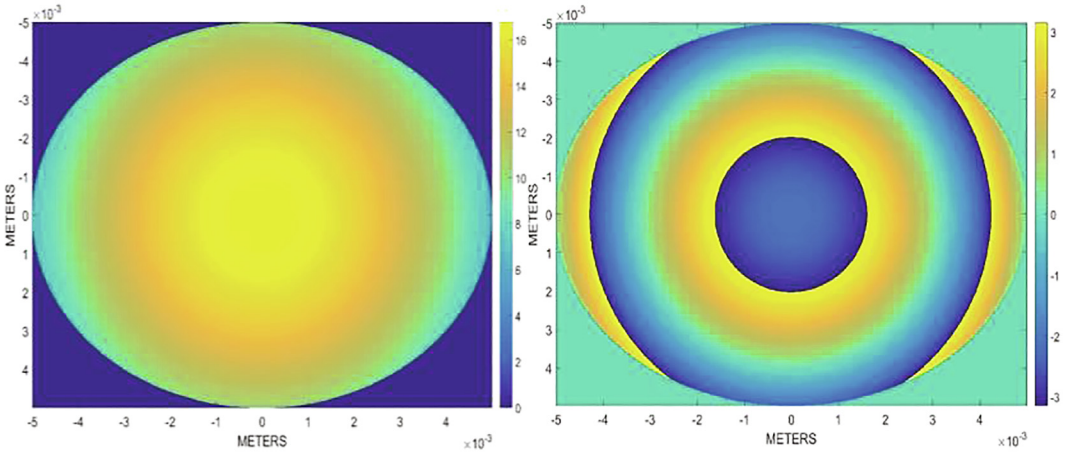

Fig. 10. Images of the unwrapped and wrapped phase recovered from the averaged negative defocus image. The color bar on the side is in units of radians demonstrating significant potential for phase wrapping.

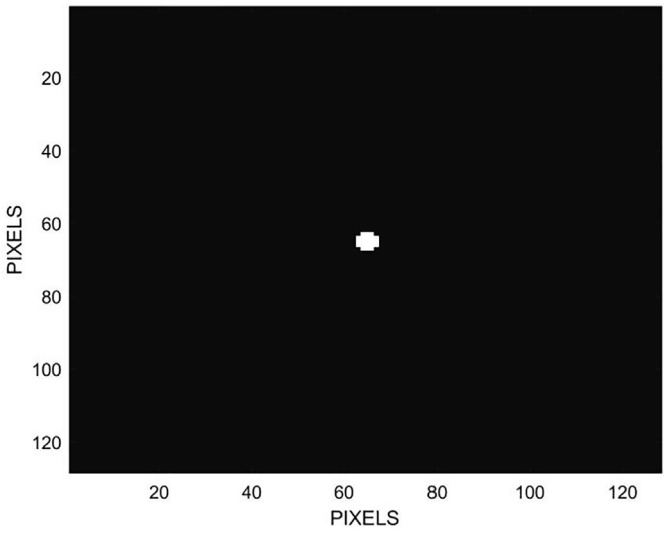

Fig. 11. Image of the reconstructed image of the pinhole.

Tables 2 and 3 show the average result obtained by the algorithms for each Zernike coefficient.

Table 4 reports the aberration coefficient variance when processing the 200 frames of image data. The frames were processed 2 at a time, $J = 2$, with one positive defocus image and one negative defocus image. 100 sets of 2 frames were processed to produce coefficients for each set.

Figs. 9 and 10 show the recovered unwrapped phase across the pupil for the negative and positive focus positions side by side with their wrapped phase counterparts using the ZIPPER algorithm. These images demonstrate the significant phase wrapping present in the pupils of the imaging systems.

The ZIPPER algorithm provides the most precise and accurate phase retrieval approach of the two approaches studied in this paper. Fig. 11 shows the image of the pinhole reconstructed from the algorithm as well.

6. Conclusions

The ZIPPER algorithm achieved superior performance over traditional GS phase retrieval combined with a state-of-the-art phase unwrapping algorithm when utilized in a blind deconvolution algo-

rithm and attempting to unwrap the phase at every iteration. This was achieved by producing differential phase estimates from each iteration of the GS algorithm combined with the incremental progression of the blind deconvolution algorithm. This allowed the new Zernike-based phase unwrapper to "keep up" with the changes, all the while accumulating phase changes that would, if taken all together, cause wrapping around the unit circle.

The new Zernike-based phase retrieval algorithm also outperformed the CPULSI phase unwrapper during the incremental phase retrieval steps. This is most likely due to the new unwrapper's design for computing continuous phase functions being based on the Zernike polynomials themselves as opposed to satisfying other continuity constraints.

Future research will apply the new algorithm for recovering images in single-frame blind deconvolution scenarios, since the phase is carefully constrained in the pupil, the hope is that the trivial solution to the blind deconvolution problem can be avoided through this parameterization.

7. Disclaimer

The opinions and views expressed by the author are not necessarily those of the United States Department of Defence or the United States Air Force.

Declaration of Competing Interest

The authors declare that they have no known competing financial interests or personal relationships that could have appeared to influence the work reported in this paper.

Acknowledgements

This work was funded by the United States Air Force Office of Scientific Research.

References

Fienup, J.R., 2013. Phase retrieval algorithms: a personal tour [Invited]. Appl. Opt. 52 (1), 45–56.
Gerchberg, R.W., Saxton, W.O., 1972. A Practical Algorithm for the Determination of Phase from Image and Diffraction Plane Pictures. OPTIK 35 (2), 237–246.
Roddier, F., 1988. Curvature sensing and compensation: a new concept in adaptive optics. Appl. Opt. 27 (7), 1223–1225.
Krist, J.E., Burrows, C.J., 1995. Phase-retrieval analysis of pre- and post-repair Hubble Space Telescope images. Appl. Opt. 34 (22), 4951–4964.
Ghiglia, D.C., Pritt, M.D., 1998. Two-dimensional phase unwrapping theory, algorithms and software. Wiley-Interscience, Hoboken.
Xia, H., Montresor, S., Guo, R., Li, J., Yan, F., Cheng, H., Picart, P., 2016. Phase calibration unwrapping algorithm for phase data corrupted by strong decorrelation speckle noise. Opt. Express 24 (25), 28713. https://doi.org/10.1364/OE.24.028713.
Paxman, R.G., Schulz, T.J., Fienup, J.R., 1992. Joint Estimation of Object and Aberrations Using Phase Diversity. J. Opt. Soc. Am. A 9 (7), 1072–1085.
Woods, D., 2012. The Space Surveillance Telescope: Focus and Alignment of a Three Mirror Telescope. Advanced Maui Optical and Space Surveillence Technologies Conference, Maui.
Hickson, P., 1994. Wave-front curvature sensing from a single defocused image. J. Opt. Soc. Am. 11 (5), 1667–1673.
Tokovinin, A., Heathcote, S., 2006. Donut: Measuring Optical Aberrations from a Single Extra focal Image. Astronomical Soc. Pacific 118 (846), 1165–1175.
Zingarelli, J.C., Cain, S.C., 2013. Phase retrieval and Zernike decomposition using measured intensity data and the estimated electric field. Appl. Opt. 52 (31), 7435–7444.
Hecht, E., 1990. Optics. Addison-Wesley, Menlo Park, CA.
Goodman, J.W., 1968. Introduction to Fourier Optics. McGraw-Hill, New York.
Cain, Stephen C., 2020. Non-linear statistical photocalibration of photodetectors without calibrated light sources. Appl. Opt. 59, 2767–2775.
Schulz, T.J., 1993. Multiframe blind deconvolution of astronomical images. J. Opt. Soc. Am. A 10 (5), 1064–1073.
Dempster, A.P., Laird, N.M., Rubin, D.B., 1977. Maximum Likelihood from Incomplete Data via the EM Algorithm. J. R. Stat. Soc. Ser. B (Methodological) 39 (1), 1–38.
Shepp, L.A., Vardi, Y., 1982. Maximum Likelihood Reconstruction for Emission Tomography. IEEE Trans. Med. Imaging 1 (2), 113–122.
Bartelt, Bryan R., 2020. Global Gradient-Based Phase Unwrapping Algorithm for Increased Performance in Wavefront Sensing, AFIT thesis, March 2020.